Customized biochar for soil applications in arid land: effect of feedstock type and pyrolysis temperature on soil microbial enumeration and respiration

Ahmed Al-Rabaiai[a], Daniel Menezes-Blackburn[a,*], Said Al-Ismaily[a], Rhonda Janke[b], Bernhard Pracejus[c], Ahmed Al-Alawi[d], Mohamed Al-Kindi[e], Roland Bol[f]

a Department of Soils, Water and Agricultural Engineering, Sultan Qaboos University, P.O. Box 34, Al-Khoud 123, Muscat, Sultanate of Oman

b Department of Plant Sciences, Sultan Qaboos University, P.O. Box 34, Al-Khoud 123, Muscat, Sultanate of Oman

c Department of Earth Sciences, Sultan Qaboos University, P.O. Box 36, Al-Khoud 123, Muscat, Sultanate of Oman

d Department of Food Sciences and Nutrition, Sultan Qaboos University, P.O. Box 34, Al-Khoud 123, Muscat, Sultanate of Oman

e Department of Pathology, Sultan Qaboos University, P.O. Box 35, Al-Khoud 123, Muscat, Sultanate of Oman

f Institute for Bio and Geosciences, Agrosphere (IBG-3), Forschungszentrum Jülich, Wilhelm-Johnen-Straße, 52428 Jülich, Germany

* danielblac@squ.edu.om

Abstract:

Biochar is rapidly gaining worldwide interest as an agro-technology for increasing soil health and carbon storage. This study investigated the physicochemical characteristics and impact on soil microbes of biochar amendments from three feedstock sources: date palm leaves (D), mesquite plants (M) and sludge compost (S.C.); pyrolyzed at 450 °C, 600 °C and 750 °C. Scanning electron microscopy images showed an apparent pore size increase with increasing pyrolysis temperature. The increase in pyrolysis temperature decreased O-H and C-O bonds and increased the proportion of C-C bonds, as obtained from the Fourier transform infrared spectroscopy studies. Thermostability was highest at a pyrolysis temperature of 750 °C, with distinct thermal decomposition profiles for each of the three feedstock materials used, as indicated by the dynamic thermal gravimetric analysis. The SC biochars showed the highest mineral content (45-66%) with significantly higher water-soluble and total concentrations of mineral elements. The SC samples also showed the presence of possible soil contaminants such as Pb and As, and its use as a soil amendment is not recommended, even though the SC at 450 °C was the only nonalkaline biochar in this study. The M feedstock produced biochar with the highest surface area (600 m^2 g^{-1}) and carbon content based on loss on ignition (94.98%); nevertheless, the M biochar reduced soil microbial enumeration and respiration. This reduction increased with increasing pyrolysis temperature. Therefore, the M biochar feedstocks are not recommended for improving soil health and may be tested in the future as a microbial inhibitor for soil-borne plant pathogens. Considering the physicochemical properties and the biochar impact on soil, D at 600 °C was the best biochar selected for further studies as a soil amendment. The large differences in biochar physicochemical properties and their effect on soil microbes observed in this study suggest that the feedstock type and pyrolysis temperatures must be considered during biochar amendment production for improving soil health in arid-land agroecosystems.

Keywords: Soil health; Biochar pyrolysis; Organic waste; Mesquite stress; Feedstock quality.

1. Introduction

Significant improvements in agricultural management are required to achieve more productive and sustainable agricultural systems and to develop fragile rural economies. The adoption of effective agricultural management practices with long-term impacts is essential to maintaining and improving the sustainability of agroecosystems [1]. Many soil properties (such as ion exchange, soil organic matter, and water holding capacity, among others) can be contrived to increase the sustainability of agroecosystems, soil quality, and soil fertility and enhance water use efficiency (WUE) [2]. Biochar is one of the amendments that can improve many of these soil properties [3] and enhance agricultural productivity and sustainability [4]. Biochar soil amendments increase crop yields primarily by improving fertilizer use efficiency, water holding capacity, soil structure, and plant available water [5]. Biochar usage has been recognized as a safe solution and a viable way to improve soil quality and reduce the bioavailability of heavy metal contaminants [6]. In tropical conditions, the breakdown of noncharred soil organic amendments such as compost is rapid, and biochar represents an alternative soil-stable amendment option with a long-lasting impact on soil properties [7]. The combined application of compost and biochar shows a synergistic effect on increasing soil nutrient status and water-holding capacity [8] and stabilizing soil structure [9, 10].

Biochars are solid, carbon-rich, value-added charcoal-like amendments produced by heating biomass residues from agriculture, forestry, livestock and other carbon-rich materials under minimal oxygen supply and temperatures ranging between 300 °C and 1000 °C [5]. The biochar synthesis process consists of three stages: prepyrolysis, main-pyrolysis, and the generation of carbonaceous soil products [11]. The first stage (from room temperature to 200 °C) eliminates the moisture and light volatiles. Moisture evaporation creates hydroperoxide, –COOH, and –C.O. groups [12]. The rapid devolatilization and decomposition of hemicelluloses and cellulose start in the second stage, from 200 °C to 500 °C [13]. The breakdown of lignin and other organic materials with strong chemical bonds is achieved in the final stage over 500 °C [12].

Pyrolysis, hydrothermal carbonization, gasification, flash carbonization, and torrefaction are among the common thermochemical methods used for biochar formation [14]. Pyrolysis is the most widely used process for producing and transforming biomass into biochar [15]. After pyrolysis, the feedstock condenses aromatic structures with different shapes, including turbostratic C, amorphous C and graphite C [16]. Pyrolysis duration, temperature, and feedstock type are expected to affect the composition and physicochemical properties (pH, specific surface area, pore size, cation exchange capacity (CEC), volatile matter, ash and carbon content) of biochar [15, 17]. Higher temperatures increase the specific surface area, porosity, and carbon stability; the functional groups progressively disappear, leaving a more refractory material with an aromatic polycyclic structure [18].

Biochar manufacture and application for enhancing soil fertility is an ancient technique practiced by farmers in India, Europe, China, Japan, and America [19]. The use of biochar in agriculture has captured the interest of researchers since the discovery of Terra Preta anthropogenic soil in the Amazon River Basin in Brazil [20]. The Terra Preta soil has over 70% higher charcoal and organic matter content than nearby soils, rendering it highly productive for agriculture [5].

The most noteworthy potential benefits of biochar amendments are due to their recalcitrant nature, acting as long-term soil health conditioners and contributing to soil C sequestration and the reduction of greenhouse gas (GHG) emissions [1, 4, 21, 20]. Biochar has been shown to reduce the emissions of nitrous oxides and methane, making its application to agricultural lands an attractive approach for mitigating the adverse effects of agriculture on climate change [22]. Adding biochar alleviates the negative impact of salinity through its high sorption capacity, increasing plant growth and yields in saline soil conditions [23].

The most significant factor driving the effectiveness and economic viability of a biochar production strategy is the availability of high C:N organic wastes suitable as biochar feedstocks. However, biochar products originating from different feedstocks and pyrolysis conditions differ greatly in their amendment value and soil impact. Therefore, each potential feedstock needs to be characterized under different pyrolysis conditions for optimal soil amendment use [19]. In this study, date palms (*Phoenix dactylifera*), mesquite trees (*Prosopis juliflora*) and sludge compost were chosen because of their high abundance and environmental concerns. Date palm orchards occupy 35% of Oman's total agricultural area [24] and are similarly widespread in Southwest Asia and North Africa. Date palm fields produce approximately 152,000 tons of organic waste annually in Oman (Barreveld, 1993), which is commonly burned to ash in open farms [25], creating smoke and lowering air quality. Mesquite plants are invasive species of serious ecological, economic and social concern worldwide [26, 27]. Sewage sludge is an organic waste byproduct of wastewater treatment in most major cities worldwide [28] and is often composted for use in agricultural soils [29]. In Oman, sludge stabilization by composting produces an average of 118 tons of organic fertilizer per annum, with low social acceptance due to its human origin [30]. Converting these organic wastes into biochar can reduce solid waste disposal in landfills and their associated environmental problems [31].

The biochar feedstocks used in this study were selected for their high abundance and/or environmental concerns. They were a) composted sewage sludge from urban wastewater treatment plants; b) stems/wood of invasive *Prosopis juliflora* plants; and c) leaves of date palms (*Phoenix dactylifera*), a dominant crop in the Middle East and North Africa. This work aimed to evaluate the effect of increasing pyrolysis temperatures (450, 600, and 750 °C) for the three selected feedstocks on the resulting biochar physicochemical properties and soil amendment value. Our underlying hypotheses are that i) both feedstock type and pyrolysis temperature will condition short-term biochar effects on soil health, here represented by soil microbial enumeration and respiration; and ii) this biochar effect on soil health can be explained by their underlying biochar physicochemical properties, driven by feedstock type and pyrolysis temperature.

2. Materials and methods:

2.1 Collection of feedstocks and biochar production

Three different feedstock materials were selected in this research, and their biochar was produced under increasing temperatures by using a laboratory muffle furnace. The feedstock used in this study was sewage treatment sludge (S.C.), which was made from human waste after tertiary wastewater treatment and then stabilized by mixing with woody materials to make compost produced by the Oman Wastewater Services Company. This compost currently has low acceptance among end-users due to its human origin. Date palm leaves (D) (*Phoenix dactylifera*) were collected from a farm located in Al Batinah South Governorate (23°55'17.1"N 57°11'07.4"E) and are widely generated every year from annual pruning. Mesquite plant (*Prosopis juliflora*) steams/wood (M) were collected from a farm located in Al Batinah South Governorate (23°55'17.7"N 57°11'07.5"E), a well-known invasive plant species in several regions around the world, with severe negative environmental impacts on local fauna and flora. Table 1 shows the general properties of the selected feedstock; hemicellulose, cellulose and lignin were identified by using the Van Soest method [32]. For the organic elemental analysis, C, H, N and S were quantified by using a CHNS analyzer (model: 2400I; Mark: Perkin Elmer).

The feedstocks were chopped to a size range from 0.5 cm to 1.0 cm to allow their compaction in the pyrolysis reactors. The chopped samples were washed with deionized water and oven-dried at 110 °C for 24 h. The SC feedstock was homogenized and compacted into the reactor without further pretreatment. Pyrolysis was carried out in vertical, tubular, stainless steel reactors. To enable only the evolved volatiles to escape, this container has a cover with a tiny vent on the lid. The chopped feedstock was compacted in the reactor and placed in the furnace (Carbolite™ CWF1113-230SN+&02-301, Fisher Scientific, New Hampshire, US) at three different temperatures (450 °C, 600 °C and 750 °C) with a retention time of 2 hours. Once the appropriate temperature was reached, compacted raw samples in the cylinder were placed in the heated furnace. When the retention time was completed, containers were immediately removed, covered with aluminum foil to avoid further char oxidation, and allowed to cool at room temperature (~23 °C). The mass loss between the raw oven-dried (105 °C) biomass and the final product was used to calculate the biochar yield during the experiment, defined as the ratio of biochar mass to feedstock mass [33].

Table 1. General properties of the selected feedstock used for the production of biochar (D = date palm leaves; M= mesquite plants; SC= composted sludge from water treatment plants). The contents of hemicellulose, cellulose and lignin were identified by using the Van Soest in 1963 method. Means are followed by the standard deviation (±SD, n=3)

Feed-Stook	**Hemicellulose (%)**	**±SD**	**Cellulose (%)**	**±SD**	**Lignin (%)**	**±SD**	**C%**	**±SD**	**H%**	**±SD**	**N%**	**±SD**
D	14.21	0.15	51.05	0.32	4.23	0.21	41.69	0.28	5.78	0.47	2.33	0.34
M	11.71	0.20	53.95	0.41	13.20	0.21	44.37	0.26	6.37	0.58	1.77	0.56
SC	n.d	n.d	35.42	1.60	18.66	0.73	31.64	0.89	3.79	0.27	5.05	0.63

Feed-Stook	**S%**	**±SD**	**LOI (%)**	**±SD**	**Moisture (%)**	**±SD**	**pH**	**±SD**	**EC**	**±SD**
D	0.79	0.05	94.43	0.17	3.96	0.47	6.5	0.00	3.23	0.02
M	0.46	0.07	97.56	0.04	3.60	0.18	5.6	0.00	1.38	0.05
SC	0.89	0.07	52.24	0.40	2.20	0.14	7.1	0.01	3.78	0.06

n.d (not detected); C%= carbon; H%= hydrogen; N%= nitrogen; S%= sulfur; EC (dS m^{-1}) = Electrical conductivity; LOI (%) = organic matter loss on ignition.

2.2 Physical and chemical characterization of biochar

Biochar characterization was performed as described by Singh [34] and Rajkovich [35]. The biochar pH, electrical conductivity (E.C.), and bulk density was measured using a 20:1 water:biochar (mL:g) ratio, pH and E.C. of biochar was determined using a triplicate subsample. Samples were shaken for 2 hours for equilibrium before pH (Jenway, UK, Barloworld Scientific Ltd. Model: 3510) and E.C. (Thermo Scientific™, UK; model: Orion star 212) measurements were taken in the supernatant above the settled biochar. The bulk density (mass/volume) was assayed using dried biochar (at 80 °C) filled to the appropriate capacity in a 25 mL glass volumetric cylinder. The bulk density was used to calculate the total biochar porosity, and the biochar particle density was assumed to be 0.570 g cm^3 for all biochar products [36].

The specific surface area (m^2 g^{-1}) was assayed by sorption ethylene monoethyl ether (EGME) according to Cerato and Lutenegger [37]. Namely, 1 g of each sample (oven-dried at 110 °C) was saturated with EGME buffer, and the excess EGME was evaporated in a vacuum desiccator. The weight of the adsorbed EGME monolayer (0.000286 g m^{-2}) was used to calculate the specific surface area of the biochar samples.

Loss on ignition (LOI) was measured for biochar samples following Koide [38] based on the relative residual mass of oven-dried samples (at 105 °C for 24 h) after burning at 550 °C for 4 hours in a muffle furnace (Carbolite™ CWF1113-230SN+&02-301, Fisher Scientific, New Hampshire, US).

The cation exchange capacity (CEC) for 2.5 g biochar samples was measured by saturation with sodium acetate (25 ml of 1 *N* NaOAc). The mixture was kept in an orbital shaker (5 minutes 100 rpm) and centrifuged (5 minutes at 5000 g), and the supernatant was discarded. The saturation with sodium acetate step above was repeated. The samples were then washed with 25 mL of ethanol (5 minutes 100 rpm) and centrifuged (5 minutes 5000 g), and the supernatant was discarded. The ethanol wash step above was repeated. Then, ammonium acetate (25 mL of 1 *N* NH_4OAC) was added, shaken (5 minutes 100 rpm), and centrifuged (5 minutes 5000 g), and the supernatant was filtered and collected. The elution step was repeated, and the supernatant was determined in a flame photometer. Exchangeable sodium cations were assayed and used to calculate the CEC [39].

2.2.1 Soluble and total elemental analysis

The total elemental content of the biochars for elements heavier than Na was quantified using X-ray fluorescence energy dispersion spectroscopy (ED-XRF, Niton XL3t GOLDD Thermo, U.K.). Containers made of polypropylene were filled with biochar samples to a height of 20 mm, and the tops were sealed with a polypropylene sheet of 4 µm thickness (Premier Lab Supply model TF-240-255). Each sample was assayed over 180 seconds. Triplicate samples were examined. Water-soluble elemental composition was measured using inductively coupled plasma–optical emission spectrometry (ICP–OES, Model: 8000 DV). Deionized water extraction was performed using a 20:1 water:biochar (mL:g) ratio, and samples were shaken horizontally for 24 hours and then filtered for analysis.

2.2.2 Biochar functional group characterization

The biochar surface functional groups were assessed using Fourier transform infrared spectroscopy (FTIR) (Agilent Technologies, U.S.; model: Cary 670 series FTIR) equipped with a mercury-cadmium-telluride (MCT) detector fitted with an attenuated total reflection (ATR) accessory (Gladi ATR from Pike Technologies, WI, USA). Before analysis, biochar samples were oven-dried at 105 °C and ground. To acquire the spectra, 36 scans in wavelengths ranging from 400 to 4000 cm^{-1} were used.

2.2.3 Biochar thermostability

The thermal stability of the biochars was analyzed by thermogravimetric analysis (TGA). Namely, the mass change of raw materials and biochars as a function of temperature was evaluated using SDT Q600 TGA equipment (SDT Q600 V20.9 Build 20, Module, DSC-TGA Standard, InstSerial, 0600-0868, USA) under a nitrogen atmosphere. Approximately 10 mg of each biochar sample was weighed into an aluminum crucible and subjected to TGA analysis using a nitrogen flow of 100 $mL\cdot min^{-1}$ and a heating rate of 10 °C·min−1 from 50 °C to 600 °C.

2.2.4 Scanning electron imaging of biochar

Scanning electron microscopy (SEM) was used to examine the porous microstructure of the biochar using a Jeol scanning electron microscope (JEOL Ltd, Japan; Model: JSM -– 5600

LV). In addition, we assessed the changes in the physical shape of the biochar surface treated at different temperatures during pyrolysis. For each sample, particles were mounted on a 10 mm diameter aluminum stub stuck by a double side carbon adhesive (SPI, USA) and coated with a 25 nm thick gold layer (BioRad SEM coating system, U.K.) to enhance the conductivity of the biochar and to avoid charging artefacts when acquiring micrographs.

2.2.5 Effect of biochar on soil microbial enumeration and respiration

The short-term effects of biochar on the culturable heterotrophic aerobic fungi, bacteria and actinomycetes were evaluated from soil that had been incubated for one week with each of the biochar samples on agar media using the standard serial dilution plating method [40]. The sandy-loam textured soil chosen for this study was collected in the South Al Batinah region of Oman (23°35'52.7"N 58°09'50.4"E). Soil characteristics were measured and included electrical conductivity on the saturated paste extract EC_e = 8.3 dS m^{-1}, pH = 8 and 0.33% soil organic matter by the loss on ignition method. Briefly, 1.5 g of each biochar sample was mixed with 30 g (5% biochar by weight) of soil and incubated for one week at room temperature. Then, 10 g of the mixture was added to 90 mL of sterilized distilled water. After homogenization, the soil suspension was subjected to four sequential 10× dilutions in sterile 0.85% NaCl. Culturable fungi were assessed by pour-plating one mL of the soil suspensions on rose bengal agar. Culturable bacteria were assayed by spreading 100 µL of soil suspension on peptone yeast agar (PYA) medium, and for actinomycetes, glycerine casein agar (GCA) medium was used. The plates were incubated for 2-7 days at 36 °C. The accuracy of the microbial enumeration was increased by using three analytical replicates (3 agar plates for each dilution) for each of the three experimental sample replicates. The results were calculated from the direct count of colonies at the appropriate dilution of the original soil+biochar suspensions and expressed as colony-forming units (CFU g-1 of dry soil)

To study the effect of biochar on soil microbial activities, respiration assays were performed using the same one-week soil+biochar incubations (see above) using the MicroResp™ system (The James Hutton Institute, U.K.), as described by Campbell et al. (2003). Deep-well microplates (96 wells, 1.2 ml per well) were filled with incubated soil+biochar (0.58±0.03 g). Soils were further moistened with 25 µL of either sterile deionized water or a glucose solution for assessing substrate-induced respiration. A second microplate holding a CO_2 detection gel (12.5 mg kg^{-1} cresol red, 150 *mM* KCl, and 2.5 *mM* $NaHCO_3$ in 1% purified agar) was assembled on top of the soil microplate using an airtight sealing system. The system was then incubated in the dark at room temperature, and the detection plates were read after 20 hr. The absorbance of the indicator plates was measured at 570 nm using a microplate reader before and after incubation with soils. The CO_2 released from soils (% CO_2) was converted to respiration rate (μg CO_2-C g^{-1} dry soil h^{-1}) as described by Campbell [41].

2.3. Statistical analysis

Data calculations, manipulation, average, standard deviation and correlation analysis were performed using Microsoft Office Excel 2016. The data were analyzed using two-way ANOVA, and significantly different means between treatments were separated with Tukey's test at the $p \leq 0.05$ significance level using JMP13 [42].

3. Results

3.1 Effect of feedstock and pyrolysis temperature on the physicochemical properties and composition of biochar

There was a significant effect of feedstock, temperature and a statistically significant interaction of temperature and feedstock on the yield of biochar samples (ANOVA $p \leq 0.01$). The biochar yields were lowest for the M samples at 600 °C (26.7%) and highest for the S.C. samples at 450 °C (71.5%). Regardless of the feedstock type, there was a yield decline between pyrolysis temperatures of 450 and 600 °C, and no further significant yield reductions were observed between 600 and 750 °C (Tukey $p \leq 0.05$). Similar to the yields, there was a highly significant effect (ANOVA $p \leq 0.001$) *of* feedstock and temperature (and their interaction) on the LOI representing the organic matter/carbon content of the biochar samples. The LOI was lowest for S.C. samples at 750 °C (33.6%) and highest for M samples at 450 °C (94.5%). Curiously, the LOI showed no significant decline with increasing pyrolysis temperature for the D and M samples, *i.e.*, for these fully organic plant materials, as all easily combustible C is ashed at all temperatures, and their biochars have similar organic/mineral contents.

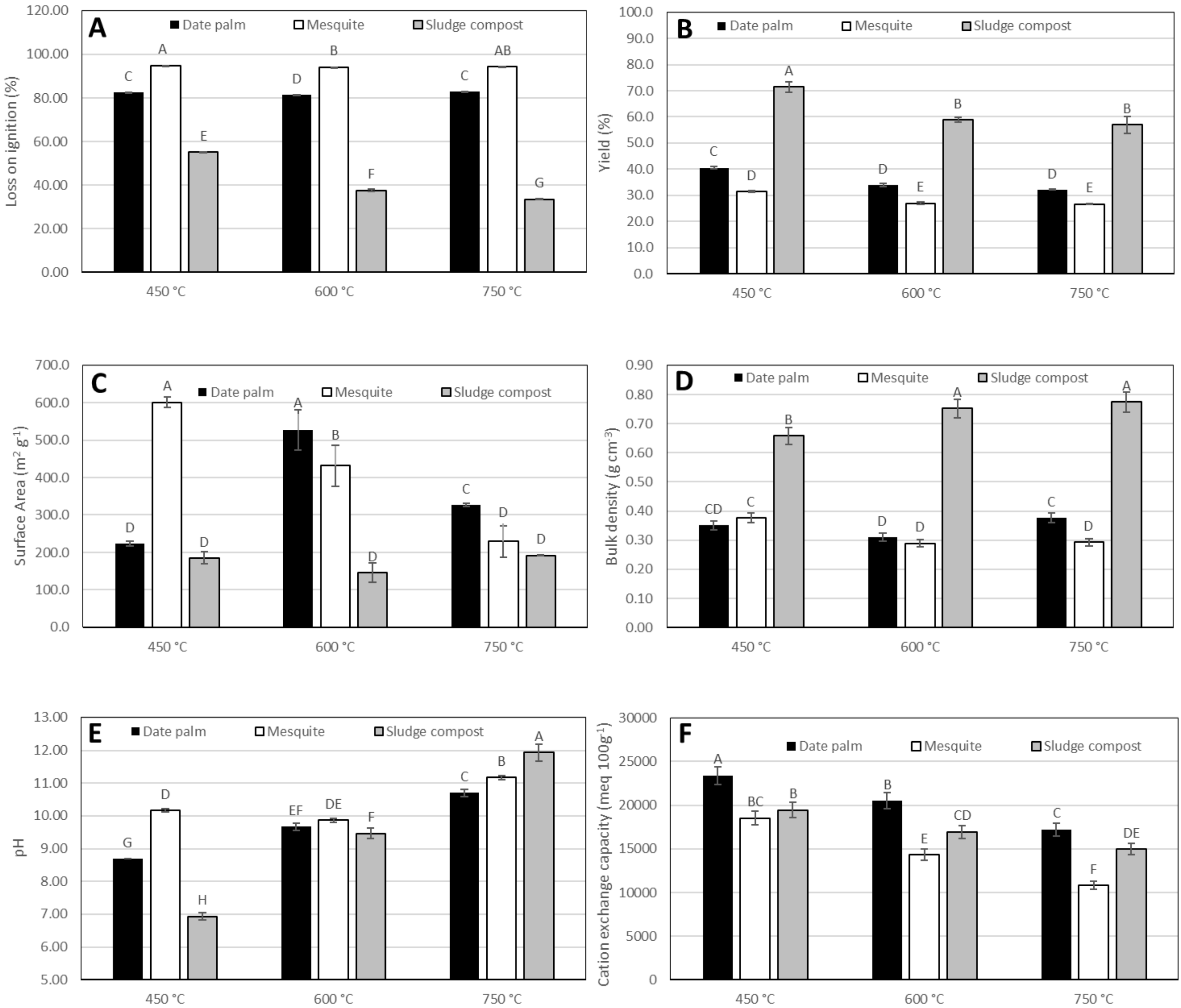

Figure 1. Physicochemical properties of biochar from different feedstocks (date palm leaves; mesquite plants; sludge compost) subjected to pyrolysis at different temperatures (450, 600 and 750 °C). Means and standard deviations (±SD, n= 3) followed by the same letter within a column are not significantly different (Tukey's test $P < 0.05$).

Biochar's physicochemical characterization (Figure 1) was remarkably different depending on the type of feedstock and pyrolysis temperatures used, with significant effects on many biochar properties. In general, S.C. samples showed the highest pH values at 750 °C (up to 11.93,

Figure 1E), yields at 450 °C (up to 71.5%, Figure 1B) and bulk density at 750 °C (up to 0.77 g cm^{-3}, Figure 1D), while D samples showed the highest E.C. at 600°C (up to 5.20 dS m^{-1}, Table S1) and CEC values at 450°C (up to 205.0 meq 100 g^{-1}, Figure 1F). The highest values for surface area at 450 °C (up to 600 g cm^{-3}, Figure 1C), total porosity at 600 and 750 °C (0.77 cm^3 cm^{-3}, Table S1) and loss on ignition at 450 °C (94.98%, Figure 1A) were observed for the M biochar samples. The pH values for all biochar samples ranged from 6.9 to 11.9 (Figure 1E). For all the feedstocks used, the pH significantly increased (*$p \leq 0.01$*) with increasing pyrolysis temperature (from 450 to 750 °C). For the D and M biochar samples, the pH was increased by 1 unit, while for the S.C. samples pH unit increased 2.4-2.5 units with increasing pyrolysis temperatures. Post hoc comparisons Tukey HSD showed that the only case where pyrolysis temperature showed no effect on the pH of biochar was between M 450 and M 600. The E.C. $_{(20:1)}$ for all biochar samples ranged from 1.04 to 5.20 dS m^{-1} but did not show any consistent trends related to the feedstock type or the pyrolysis temperature (Table S1).

The surface area of biochar was significantly affected by the feedstock type (*$p \leq 0.01$*) and pyrolysis temperature (*$p \leq 0.05$*) (Figure 1C). However, no clear trends in the surface area response to increasing pyrolysis temperatures were observed for the different feedstocks tested. The biochar surface area ranged from 146 m^2 g^{-1} to $^{600\ m2}$ g^{-1} for SC 600 and M 450, respectively. The bulk density of biochar was significantly affected by feedstock type and pyrolysis temperature and had a significant interaction effect ($p \leq 0.001$). The bulk density of the biochar decreased at higher temperatures for M and increased at higher temperatures for S.C. but had no clear trend related to temperature for D. The CEC was decreased by increasing pyrolysis temperatures.

The water-extractable elemental composition (Na, K, Ca, Mg, Al, Sr, B, Zn, Table S2) of biochar samples was, in general, significantly affected by the feedstock type (*$p \leq 0.01$*). However, the effect of pyrolysis temperature was only significant for Na, Mg, B and Zn (*$p \leq 0.01$*). The concentration of soluble cations showed a variable response, with no clear patterns observable for multiple elements across different feedstocks and pyrolysis temperatures. The highest K concentration was recorded for the D and M biochar samples. The Na and K concentrations were highest at 600 °C for the D and M biochar samples and for S.C. biochar samples at 450 °C. The Ca concentration increased with increasing pyrolysis temperatures for D biochar, whereas for M and S.C., the Ca concentration was lowest when produced at 750 °C. The highest concentration of Mg was observed for SC 450 and D 600. The Al concentration was very low for the D and M biochar samples (~ 0.1 mg.kg^{-1}) and was significantly higher for the S.C. biochar samples produced at 750 °C (3.9 $mg.kg^{-1}$). The highest concentration of Sr was recorded in the D sample pyrolyzed at 600 °C (4.6 $mg.kg^{-1}$), whereas B and Zn were highest for D and S.C. biochar samples pyrolyzed at 450 °C.

The total elemental composition of biochar samples obtained by ED-XRF is presented in Table 2 and Table S3. All detected elements of biochar samples (Ca, K, Si, P, Fe, Zn, Al, Ti, Sr, Cu, SC, Zn, Mo, Cl, Cr and Mg) were significantly affected by feedstock type (ANOVA, $p \leq 0.01$). In addition, there were significant effects of the pyrolysis temperature on the total concentrations of Si, Cl and Mg ($p \leq 0.05$). The SC biochar (and the raw feedstock) showed the highest total concentrations of most mineral elements detected by ED-XRF (Ca, P, Fe, Mg, Zn, Al, Ti, Cu, Zr, Mo). Elements of environmental concern, such as Pb, As and Cr, were only found in S.C. biochar samples at concentrations of approximately 90, 10 and 300 mg kg^{-1}, respectively. The total K and Si concentrations were the highest in the M and D biochars, respectively. When compared with their respective raw material feedstocks, in general, biochar samples did not show significant changes in the total elemental concentration (Tukey, $p \leq 0.05$), except for SC at 600 *°C* or higher.

Table 2. Energy dispersion X-ray fluorescence spectroscopy (ED-XRF) elemental analysis of biochar from different feedstocks (D= date palm leaves; M= mesquite plants; SC= sludge compost) subjected to pyrolysis at different temperatures (raw= untreated feedstock; 450. 600 and 750 °C). Means and standard deviations (±SD, n=3) followed by the same capital letter are not significantly different for different temperatures within the same feedstocks, and means followed by the same small letter are not significantly different for different feedstocks at the same pyrolysis temperatures (Tukey's test P < 0.05).

	Ca(%)	±SD		K(%)	±SD		Si(%)	±SD		P(%)	±SD		Fe(%)	±SD		Cl (%)	±SD		Mg (%)	±SD		Zn(%)	±SD	
D raw	0.78	0.02	Cb	1.91	0.03	Ca	0.91	0.01	Db	0.17	0.00	Db	0.03	<0.01	Ac	0.77	0.01	Aa	<0.01		Da	<0.01		Ab
D450	1.69	0.14	Bb	1.84	0.17	Cb	2.96	0.52	Ba	0.40	0.08	Bb	0.01	<0.01	Bb	<0.01		Db	0.12	0.12	Cb	<0.01		Ab
D600	0.78	0.10	Cc	3.51	0.05	Ab	1.33	0.14	Ca	0.27	0.02	Cb	0.01	<0.01	Bb	0.65	0.03	Ba	0.26	0.26	Ba	<0.01		Ab
D750	2.16	0.13	Ab	2.89	0.20	Ba	5.18	0.95	Aa	0.74	0.10	Ab	0.01	<0.01	Bb	0.32	0.04	Ca	0.54	0.19	Aa	<0.01		Ab
M raw	0.80	0.05	Bb	1.89	0.05	Ca	<0.01		Ac	0.14	0.01	Bb	0.11	<0.01	Ab	0.21	0.01	Bb	<0.01		Ba	<0.01		Ab
M450	1.15	0.05	Ac	4.48	0.16	Ba	<0.01		Ac	0.28	0.01	Ab	0.03	<0.01	Bb	0.19	0.01	Ba	<0.01		Bc	<0.01		Ab
M600	1.16	0.02	Aa	4.97	0.14	Aa	<0.01		Ac	0.31	0.02	Ab	0.03	<0.01	Bb	0.35	<0.01	Ab	<0.01		Bc	<0.01		Ab
M750	0.46	0.14	Cc	2.04	0.37	Cb	<0.01		Ac	0.10	0.04	Bc	n.d.	<0.01	Cb	0.08	0.03	Cc	0.08	0.08	Aa	<0.01		Ab
SC raw	4.93	0.09	Ba	1.16	0.03	Bb	2.35	0.18	Ba	1.99	0.13	Ba	1.93	0.02	Ca	0.26	0.01	Ab	<0.01		Ca	0.11	0.01	Aa
SC450	5.18	0.35	Ba	1.18	0.10	Bc	2.42	0.39	Ba	3.21	0.45	Aa	2.19	0.10	Ba	0.18	0.03	Ba	0.53	0.14	Aa	0.12	0.01	Aa
SC600	2.69	0.19	Ca	0.42	0.05	Cc	0.83	0.12	Cb	0.94	0.08	Ca	1.16	0.07	Da	0.06	0.01	Cc	0.12	0.12	Bb	0.09	0.01	Ba
SC750	7.20	0.12	Aa	1.49	0.02	Ac	3.32	0.08	Ab	3.07	0.07	Aa	2.53	0.04	Aa	0.22	0.01	Ab	0.39	0.39	ABa	0.16	0.01	Aa

3.2 Functional groups and structure of biochar through FTIR spectroscopy

The FTIR spectra of biochar samples produced at three pyrolysis temperatures (450 °C, 600 °C and 750 °C) and their respective original feedstock raw materials are shown in Figure 2. These spectra showed more than five absorption bands and therefore are categorized as a complex mixture of molecules. Most of the spectra showed five clear peaks in the region of 400-4000 cm^{-1}. The broad absorption peak at 3272 cm^{-1} in the absorption band of the 3200-3600 cm^{-1} region, corresponding to hydroxyl group stretching [43], [44], strongly decreased with increasing pyrolysis temperature for all feedstocks. This hydroxyl peak was much more pronounced in S.C. than in the D and M biochars. The peak at 2920 cm^{-1} was indicative of asymmetric and symmetric C-H stretching vibrations of methyl, methylene and methoxy groups [45], followed a similar trend as the hydroxyl peak, being more pronounced at S.C. samples and progressively decreased with increasing pyrolysis temperatures. The peaks at 1559 cm^{-1} in the region of 1550-1610 cm^{-1} represent C=C stretching vibrations and are indicative of the presence of alkenes [43]; these C=C peaks were more pronounced in D and M biochar than in S.C. and tended to increase with increasing pyrolysis temperature. The well-defined broad peak in the region of 1050-850 cm^{-1} (peak at 1034 cm^{-1}), corresponding to symmetric C–O stretching (1030–1110 cm^{-1}) [43], [46], strongly decreased with increasing pyrolysis temperature for S.C. and M biochars but not for D biochars.

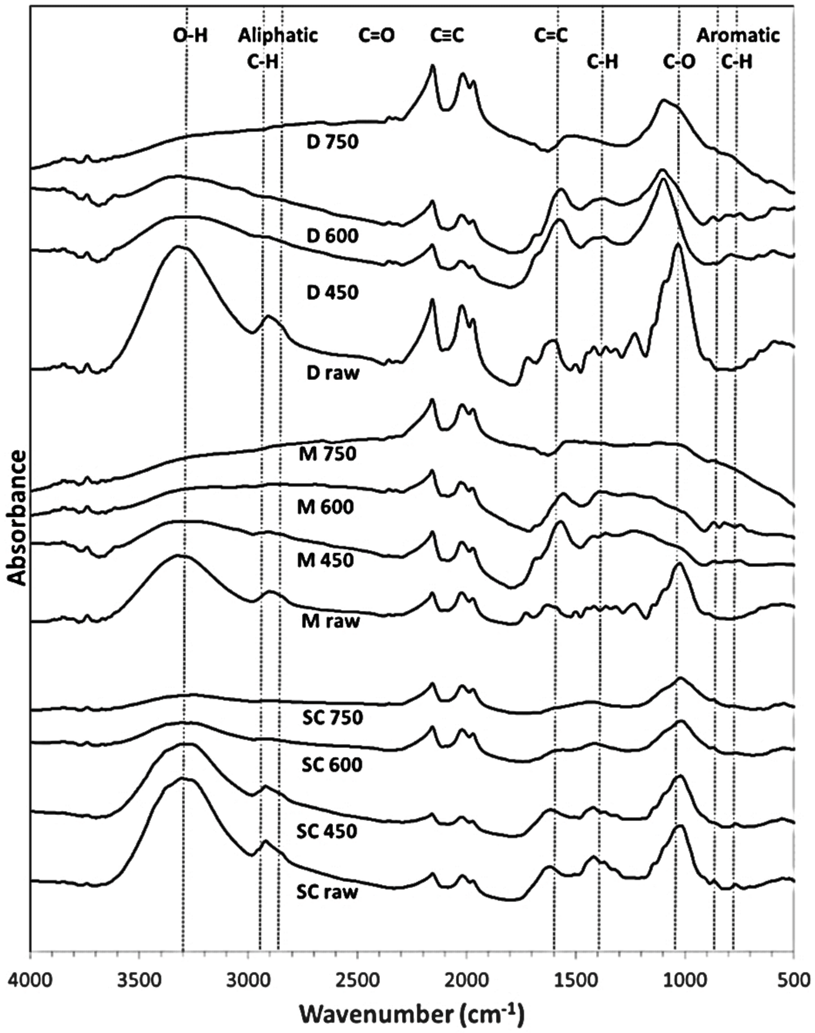

Figure 2. Fourier transform infrared spectra (FTIR) from different feedstocks (D= date palm leaves; M= mesh plants; SC= composted sludge from water treatment plants) subjected to pyrolysis at different temperatures (450 °C, 600 °C and 750 °C) and their respective original feedstock raw materials (raw).

3.3 Thermal stability of biochar

Thermal-gravimetric analysis (TGA; mass loss with increasing temperatures; Fig. 3) was used to quantify the thermal stability of different biochar samples compared to their raw feedstock materials. During the process, raw samples had more mass loss at much lower temperatures than biochar, beginning at approximately 250 °C for all raw samples, while for biochar samples, the mass loss started at 300 °C and was higher with increasing pyrolysis temperatures (Fig. 1A, 1D and 1G). Additionally, SC 750 had the highest thermal stability (63%) compared to other samples, while M 450 recorded the lowest remaining mass (8%). The slope of the mass loss curves (%/°C; Fig. 3B, 3E and 3H) showed that the D and M biochar samples showed two stages of mass loss, while the S.C. samples showed three stages of mass losses. The initial mass loss (m ~10%, T~100 °C) was variable for all samples, and the loss decreased for the biochar samples with higher pyrolysis temperatures. The second stage of mass loss began from 200 °C to 350 °C for all raw feedstock samples, and it progressively increased for all biochar samples with increasing pyrolysis temperatures. In addition, the rate of weight loss of biochar samples during this assay was more pronounced in the D and M samples than in the S.C. samples. The heat flow (w g^{-1}; Figures 3C, 3F and 3I) by differential scanning calorimetry showed how the heat capacity of samples changed during the assay; for this analysis, D and M biochar samples showed distinctively higher heat flow than S.C. samples. The heat flow increased with increasing pyrolysis temperature only for the S.C. and M biochar samples and curiously decreased for D 750 compared to D 450 and D 600.

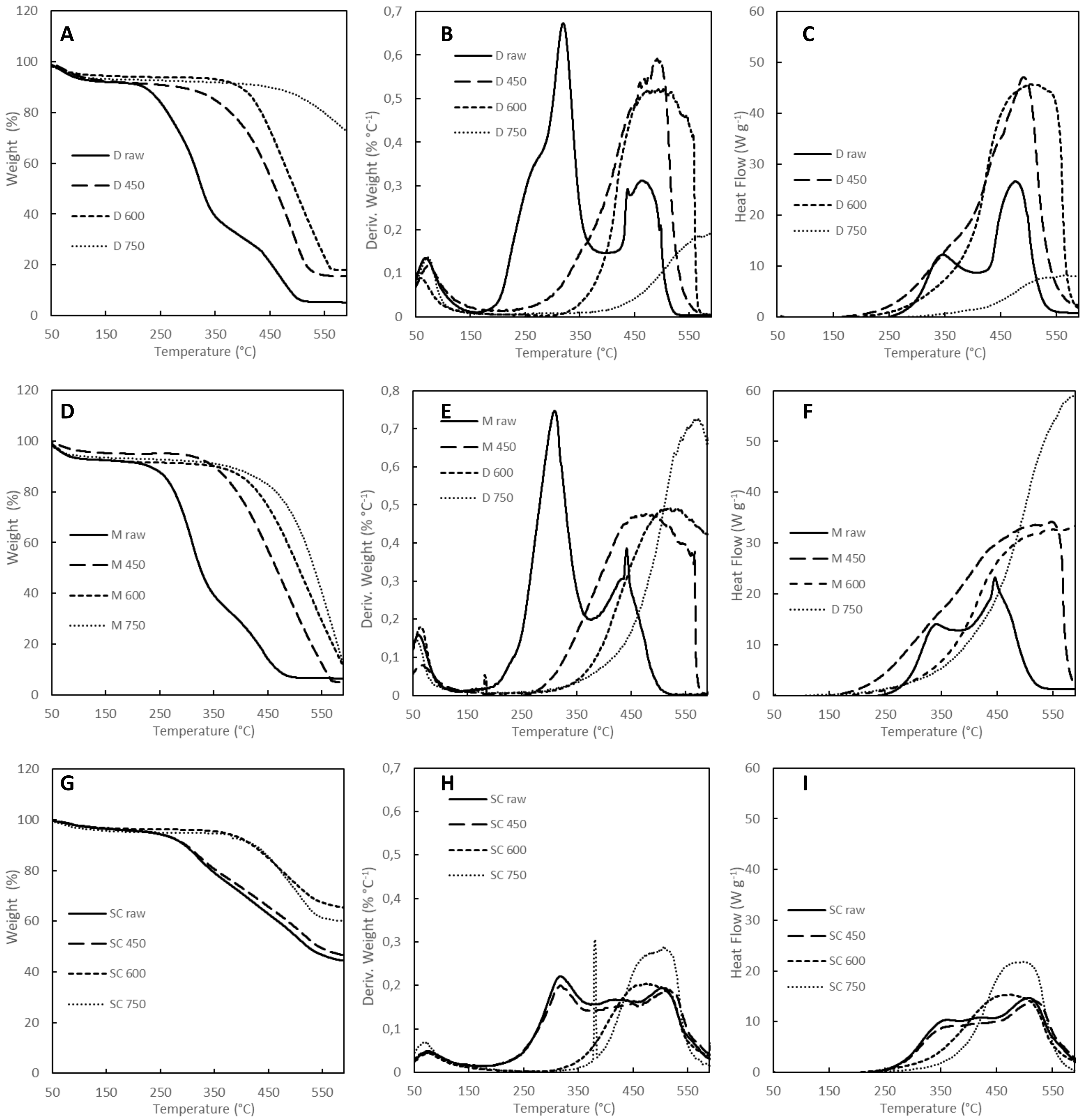

Figure 3. Thermal gravimetric analysis of biochar and raw samples for date palm leaves (first row, A; B and C), mesquite plants (second row, D, E and F) and sludge compost (third row, G, H and I) subjected to pyrolysis at 450, 600 and 750 °C. The analysis is displayed as the residual mass in % (first column, A, D and G), weight loss derivative in %/°C (second column, B, E and F) and heat flow in w/g (third column, C, F and I).

3.4 Electron microscopy of biochar microstructure

SEM micrographs of biochar samples from different feedstocks (D, M and S.C.) processed at three different temperatures (450, 600 and 750 °C) are shown in Figure 4. This analysis appeared to be heavily biased by the location where the samples were taken; therefore, it was not used as solid evidence for the conclusions drawn in this study. However, the biochar surface morphology was distinctive for the different feedstock materials. The changes appeared to be influenced by pyrolysis temperature; therefore, representative SEM micrographs are displayed to illustrate this effect. The number of micropores appeared to increased with increasing pyrolysis temperature, and the pore architecture was drastically changed. The change in the biochar pore morphology with increasing pyrolysis temperature was more apparent in D and S.C. samples than in M.

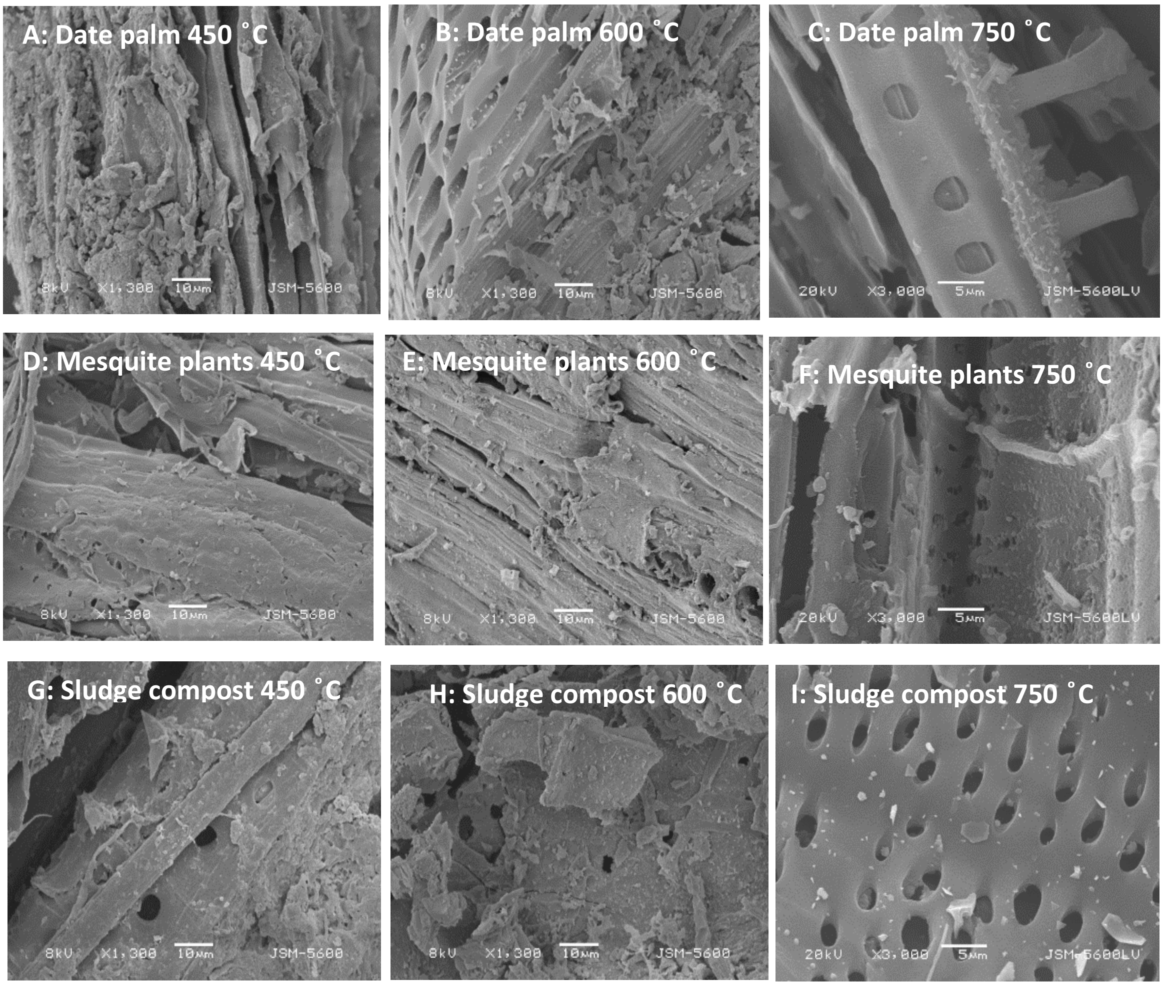

Figure 4. Scanning electron microscopy (SEM) of date palm leave biochars (A, B and C); mesquite plant biochars (D, E and F); sludge compost biochars (G, H and I); subjected to

pyrolysis at the temperatures of 450 °C (A, D and G); 600 °C (B, E and H) and 750 °C (C, F and I).

3.5 Effect of biochar on soil microbial enumeration and respiration, soil pH and EC

Soil microbial parameters were evaluated as sensitive indicators of the potential biochar impact on soil biology. The effect was measured on soils incubated for one week with 5% biochar (on a mass basis) (Table 3). The feedstock source significantly affected the enumeration of fungi (cultured in rose bengal agar), general bacteria (cultured in nutrient agar), actinomycetes bacteria (cultured in glycerol casein agar), respiration, and metabolic quotient (ANOVA, $p\leq0.001$) but not the substrate-induced respiration. The pyrolysis temperature significantly affected the enumeration of bacteria, actinomycetes, respiration, substrate-induced respiration and metabolic quotient (ANOVA, $p\leq0.001$) but not the enumeration of fungi. The enumeration of fungi was significantly increased for biochar from D and S.C. feedstocks, while for M biochar, only a few colonies were observed, and many rose bengal agar plates returned no fungal growth. The enumeration of culturable heterotrophic aerobic bacteria was significantly decreased in the D and M biochars and increased for the S.C. biochars. The enumeration of culturable actinomycetes significantly increased for D biochars and decreased for M biochars. Both general bacteria and actinomycetes bacteria significantly decreased with increasing pyrolysis temperatures, regardless of the feedstock type. From the D and S.C. biochar pyrolyzed at 450 °C, the abundances of culturable bacteria and actinomycetes were much higher than those in control soils and then decreased with increasing pyrolysis temperature. The soil microbial respiration rate (µg CO_2-C g^{-1} soil h^{-1}) and substrate-induced respiration (SIR) increased in soils amended with D and S.C. biochar pyrolyzed at 450 °C but was unaffected in soil amended with M biochars. The metabolic quotient (M.Q.; µg CO_2-C 10^6 CFU^{-1} soil h^{-1}) represents a projection of the respiration rate normalized by microbial enumeration, which was significantly increased in the M 600 and M 750 samples.

The pH and E.C. both were affected in incubated soil with biochar (5%). The effect was significant on feedstock type (ANOVA, $p\leq0.0001$).E.C. was not influenced by pyrolysis temperatures; however, soil pH was significantly ($p\leq0.0001$) increased in soils incubated with biochars that had been formed at temperatures from 450 to 750 °C.

Table 3. Changes in soil microbial parameters, pH and electrical conductivity (E.C.) after one week of incubation with 5% biochar from the different feedstock source materials (D= date palm leaves; M= mesquite plants; SC= sludge compost) subjected to pyrolysis at different temperatures (450°, 600° and 750 °C). Means and standard deviations (±SD, n=3) followed by the same capital letter are not significantly different for different temperatures within the same feedstocks, and means followed by the same small letter are not significantly different for different feedstocks at the same pyrolysis temperatures (Tukey's test P < 0.05).

	Fungi	**±SD**		**Bact.**	**±SD**		**Act.**	**±SD**		**Resp.**	**±SD**		**SIR**	**±SD**		**MQ**	**±SD**		**pH**	**±SD**		**EC**	**±SD**	
Control	9.0	1.2	Ca	51.3	6.7	Aa	51.3	6.7	Ba	1.8	0.18	Ca	4.3	0.58	Ba	1.8	0.06	Ba	7.8	0.30	Ca	0.7	0.06	Ba
D450	27.0	3.5	Aa	63.9	8.3	Ab	104.4	13.6	Ab	3.3	0.08	Ab	12.3	2.64	Aa	2.0	0.21	Bb	8.2	0.06	BCa	1.0	0.17	Aba
D600	18.0	2.3	Ba	13.5	1.8	Bb	89.1	11.6	Aa	2.1	0.09	Ba	1.8	0.08	Bc	2.1	0.18	Bb	8.6	0.15	Aba	1.2	0.09	Aa
D750	27.0	3.5	Aa	6.3	0.8	Ba	65.7	8.5	Ba	2.2	0.05	Ba	3.5	0.38	Ba	3.0	0.33	Ab	8.7	0.21	Aa	1.0	0.09	ABa
Control	9.0	1.2	Aa	51.3	6.7	Aa	51.3	6.7	Aa	1.8	0.18	Aa	4.3	0.58	Aa	1.8	0.06	Ca	7.8	0.30	Ba	0.7	0.06	Aa
M450	9.0	1.2	Ac	21.6	2.8	Bc	38.7	5.0	Bc	2.0	0.04	Ab	2.3	0.31	Bb	3.4	0.38	Ca	8.1	0.06	ABa	0.8	0.09	Aa
M600	<9	-	Bb	3.6	0.5	Cb	13.5	1.8	Cb	1.9	0.03	Aa	3.8	0.51	Aa	10.9	1.27	Ba	8.3	0.06	Aab	0.9	0.06	Aab
M750	9.0	1.2	Ac	<0.1	-	Cb	3.6	0.5	Dc	2.0	0.03	Aa	3.4	0.59	ABa	54.7	6.45	Aa	8.4	0.06	Aa	0.8	0.05	Aa
Control	9.0	1.2	Ba	51.3	6.7	Ba	51.3	6.7	Cba	1.8	0.18	Ba	4.3	0.58	Ba	1.8	0.06	Aa	7.8	0.30	BCa	0.7	0.06	Ba
SC450	18.0	2.3	Ab	259.2	33.7	Aa	250.2	32.5	Aa	11.3	1.34	Aa	11.1	0.81	Aa	2.2	0.03	Ab	7.5	0.06	Cb	1.0	0.09	Aa
SC600	9.0	1.2	Ba	34.2	4.4	Ca	81.0	10.5	Ba	2.2	0.06	Ba	2.6	0.26	Cb	2.0	0.20	Ab	8.1	0.12	Bb	0.8	0.07	Abb
SC750	18.0	2.3	Ab	39.6	5.1	BCb	36.9	4.8	Cb	1.3	0.01	Bb	1.4	0.01	Cb	1.8	0.22	Ab	8.7	0.20	Aa	0.8	0.08	ABa

Control = incubated unamended soil samples; Fungi = colony-forming units enumeration in rose bengal agar medium (x10 CFU g^{-1} soil); Bact = Bacteria colony-forming units enumeration in tryptone yeast extract agar medium (x10^4 CFU g^{-1} soil); Act. = Actinomycetes bacteria colony-forming units enumeration in glycerol casein agar medium (x10^4 CFU g^{-1} soil); Resp. = soil microbial respiration rate (µg CO2-C g^{-1} soil h^{-1}); MQ = metabolic quotient (µg CO2-C 10^6 CFU^{-1} soil h^{-1}); EC = electrical conductivity (dS m^{-1})

4. Discussion

4.1 Effect of feedstock and pyrolysis temperature on the physicochemical properties and chemical composition of biochar

The biochar pH values for all feedstocks were generally alkaline and increased with increasing pyrolysis temperature (from 450 to 750 °C), except for SC 450, which was nearly neutral. This effect has been previously reported [47], [48] and was attributed to the formation of carbonates and inorganic alkalis [13], [49]. This increase in pH was also related to changes in oxygen functional groups that occur during the pyrolysis process, with the significant removal of acidic functional groups (–COOH) and the concomitant development of basic functional groups [46], [50]. Zhang [51] reported that the separation of alkali ions from organic molecules as the pyrolysis temperature rises was the main factor responsible for increasing biochar pH values. As with our sludge compost biochars (S.C. samples), Hossain [52] showed that at low pyrolysis temperatures (300 and 400 °C), the biochar from sludge was acidic, with its pH increasing with increasing pyrolysis temperatures. This effect is attributed to the breakdown of cellulose and hemicelluloses occurring at temperatures between 200 °C and 300 °C, leading to the production of organic acids and phenolic compounds that reduce the biochar pH at low pyrolysis temperatures [53]. Alkaline ash formation was also reflected in the E.C. values, which increased with increasing pyrolysis temperatures. Our findings are in agreement with those of Pradhan [54], who showed that E.C. strongly varied in response to feedstock types and conversion temperatures.

Unsurprisingly, the yield of biochar products decreased with increasing pyrolysis temperatures. The mass loss at pyrolysis temperatures up to 450 °C is attributed to the degradation of lignocellulosic materials, water vapor emission, and loss of volatile compounds [55]. Liu [56] reported that during the pyrolysis stage, volatile matter (e.g., H_2O, CO_2, CO, NH_3, HCN, and $C_xH_yO_z$) is progressively released, resulting in lower biochar production. At higher temperatures, the emissions of carbon-rich $C_xH_yO_z$ compounds from the biochar samples are dramatically reduced, while other carbon compounds (e.g., C.O. and CO_2) are continually released. The yield reduction at higher pyrolysis temperatures can therefore be explained by the fact that most carbonization occurs during the early stages of heating [57]. The variation in the biochar yield among the selected feedstocks may be due to the dissimilarity in the amount of cellulose, hemicellulose, and lignin. Hassan [58] indicated that the yields of biochars are affected mainly by the lignin percentages of the feedstocks and the pyrolysis temperature. Lignin has a more complex structure, resulting in a long degradation process, and thus, lignin thermal degradation occurs over a wide temperature range [59]. The lignin content our feedstock material used was 4% for D, 13% for M and 19% for SC, which may explain its higher yields. Feundries D and M showed over 50% cellulose, much higher than the 35% observed for SC.

Pyrolysis temperature and feedstock sources are the major factors that determine the surface area of biochars [60]. The observed surface area increase during pyrolysis is likely due to the degradation of cellulose and hemicelluloses in the feedstocks (Table 1) as well as the creation of the channel structures observed in the SEM images [61]. Hemicellulose is broken down at temperatures ranging from 200 to 450 °C, and cellulose breakdown processes occur predominantly between 300 and 450 °C [62]. In general, a higher lignin concentration results in a higher surface area and porosity in biochar [63]. In the D samples, the surface area increased from 450 to 600 °C and then decreased at the highest pyrolysis temperature due to the formation of ash, which reduced microporous formation, lowering the surface area. This behavior is consistent with results published by Fernandes [55]. For SC biochar samples, the relatively lower surface area was not affected by pyrolysis temperature, likely due to its high mineral content. The strong reduction in surface area for M biochar samples with increasing pyrolysis temperatures may be due to the evolution of secondary reactions of primary volatiles, which, according to Lu [64], agrees with our finding that the surface area was reduced at 600 °C, as well as the loss of lignin from this woody material, as shown in the general properties in Table 1.

The micropore structure of the biochar samples was observed by SEM microscopy. The number of pores with various sizes and architectures developed due to dehydration and volatilization of the raw materials [13, 65, 66]. The reduction in the number of pores of D750 and M750 may be due to similar phenomena observed by Ben Salem [67], which showed that when the pyrolysis temperatures exceed a particular limit, the pores expand and may merge due to the decomposition of the hemicellulose, cellulose and lignin contents (Table 1). In this situation, the walls of the pores became weaker and could easily be damaged, leading to fewer pores and a higher ash content. Fernandes [55] noticed that at high pyrolysis temperatures, the structures became thinner owing to the creation of ash content, which affected the production of microporous structures.

Biochar loss-on-ignition (or organic carbon) depends on the initial mineral content of the feedstock material and the biochar yield during biochar production. Therefore, this parameter was strongly affected by the feedstock and pyrolysis technique employed [68]. Our results showed similar organic contents for the D and M biochars at pyrolysis temperatures from 450 °C to 750 °C due to the loss of moisture, carbon, and other constituents [69]. The lowest amount of organic matter detected was in the S.C. samples due to its higher mineral content [70].

The CEC represents biochar's ability to hold and store cations, one of its most beneficial properties as a soil amendment. Our results showed a consistent decrease in the CEC with increasing pyrolysis temperature for all biochar feedstocks. This reduction in CEC might be attributed to the loss of surface functional groups and the increase in carbon aromaticity [71]. Our results agree with Shaaban [72] and Guizani [73].

The water-soluble cations quantified by ICP–OES showed that the type of biomass used for biochar has a direct effect on most detected basic cations, while the temperature of the pyrolysis effect varied for different cations and different feedstocks used. The most abundant water-soluble elements detected were Na, K, Ca and Mg, which agrees with the study by Jha [74]. Saletnik [75] showed that the increase in pyrolysis temperatures and retention times had a significant influence on the concentration of the analyzed elements. The increase in pyrolysis temperature causes mineralized Ca and Mg to be released as insoluble inorganic compounds, likely via the formation of new minerals. This effect was accompanied by a pH increase, attributable to the release of basic cations [76], [77].

The studied biochar showed a rich mineralogical composition in the solid phase ED-XRF elemental analysis. Due to the loss of organic compounds (LOIs), the total Ca, K, Si, P, Fe, Mg, Zn, Al, Ti, Cu, and SC concentrations (ED-XRF) increased with increasing pyrolysis temperature compared to the raw product sample. This finding is in agreement with Waqas [78], who showed temperature thresholds for this mineralization effect. The SC biochars showed higher total concentrations of several elements, such as Al, Ti, Cu, Si, Pb, Cr, SC, Zr, and As, due to the unknown source of the sludge. Further work is needed to test the risk of using this biochar containing elements of concern, such as Pb, As, SC and Zr.

4.2 Biochar chemical structure and stability

The amount of carboxyl, hydroxyl, and amino groups, which are responsible for sorption processes in biochar samples, were reduced as the pyrolysis temperature increased compared to the feedstocks, as shown in Figure 4 ($1_{a,b,c}$). These results are in agreement with those reported by Sizirici [79]. Numerous functional groups found in feedstocks and biochar samples, such as oxygen-containing functional groups, can influence surface reactions, such as hydrophilicity and electrical and catalytic properties [80]. The FTIR spectra of all biochar samples indicated a reduction in the stretching of O–H and C–H and a reduction in functional groups with increasing pyrolysis temperatures. In other words, when produced at high temperatures, the resistance to degradation of the alcoholic, phenolic, and H-bonded hydroxyl groups decreased. These results agree with similar previous studies [16], [45], [81], [82], arguing that the intensity of the hemicellulose and lignin bands is considerably reduced due to the breakdown of the ester linkages of the carboxylic groups of lignin and/or hemicellulose. There were clear differences for all spectra in the intensity of the observed peaks with increasing pyrolysis temperature. The transformation was more evident in the sludge compost than in the date palm and mesquite biomasses, with the intensity of the O–H stretching of the hydroxyl groups and the C–H stretching of the aliphatic vibration groups being strongly reduced [83]. Pyrolysis at higher temperatures reduced the intensity of the bands in the 1000-1200 cm^{-1} region, which is attributed to oxygenation group loss hemicelluloses [84]. The FTIR data indicated that higher pyrolysis temperatures decreased the content of O- functional groups and, therefore, the reactivity of biochar, increasing biochar stability [85].

The thermal oxidative stability of the biochars was evaluated by thermogravimetric analysis (TGA), further demonstrating that the temperature of pyrolysis is an important factor when considering the stability of biochars [86]. In this regard, the higher the pyrolysis temperatures are, the higher the observed thermal stability of the biochar. As expected, mass loss was higher at lower pyrolysis temperatures [50], [87]. Li and Chen [88] stated that hemicellulose and cellulose degradation occurs in the temperature range of 200–400 °C, while the weight loss at temperatures ranging from 370 °C to 550 °C can be attributed to the thermal decomposition of lignin [89]. In the present study, the weight loss of the D and M samples was higher than that of the S.C. samples due to the higher mineral content in the latter. Thus, it can be concluded that all our tested feedstocks have a similar pattern in the thermal stability of the resulting biochar [90]. Pyrolysis temperature played a significant role in the thermal oxidation of biochars, and weight loss patterns were comparable to those observed by Onorevoli [76] and Al-Wabel [50].

4.4 Effect of biochar on soil microbial enumeration and respiration

Heterotrophic aerobic microbial enumeration is used here as a proxy for microbial biomass, and the respiration rate of the incubated soils represents the activity of the soil ecosystem, which is directly related to soil organic matter breakdown. In the present study, the highest recorded abundance of soil bacteria and actinomycetes occurred with the biochars of the lowest pyrolysis temperatures (450 °C), indicating higher carbon bioavailability in these samples. The increased microbial enumeration with biochar amendment can be attributed to biochar's microbial stimulation compared to the control soil [91]. Z. Dai [92] noticed that producing biochar at low temperatures had a greater impact on increasing microbial biomass than biochar generated at high temperatures due to its higher C bioavailability, implying that biochar supplies C substrates for microbial growth and metabolism. Therefore, microbial stimulation, although positive in the short term, the results in a low half-life of biochar amendments in soils, defeating its purpose as a stable carbon substrate.

However, biochar amendment causes a reduction in the abundance of soil microbes at pyrolysis temperatures of 600 °C and above, which suggests that the transformation of volatile matter during the conversion to biochar leads to the generation of biotoxic compounds, which has a negative influence on the abundance of soil microbes. Our finding is in agreement with Deenik [93], who showed that volatile chemicals produced during pyrolysis conversion can diminish microbial biomass. In terms of soil health, the biotoxicity of biochar is a negative outcome, which may decrease several microbial traits, such as functional diversity, possibly decreasing the ability of soil microbes to provide ecosystem services. In addition, biochar from different feedstocks may differentially impact soil microbes. According to Luo [94], biochar created at high temperatures (600 °C) did not affect the microbial biomass due to the stability of the biochar.

In our study, the respiration rate was highest at the lowest pyrolysis temperature (450 °C), and this respiration rate was progressively reduced with increasing production temperatures. As a response parameter, respiration integrates the effect of biochar on microbial biomass and its activity. Trace amounts of water-soluble organic compounds in biochar may have priming effects in stimulating microbial activities [95]. However, for soils amended with biochar produced at 750 °C, the respiration was the lowest, especially for S.C. samples. This could be due to the concentration of heavy metals in biochar observed in the ED-XRF data, which might slow down microbial activity in the soil [96], [97]. Another possible explanation is that other parameters, such as pH, significantly changed with increasing pyrolysis temperatures and may indirectly affect microbial biomass activity. Biochar amendments are also known to affect other soil properties, with indirect impacts on soil microbes, such as structure, bulk density, porosity, water retention, infiltration rates, E.C., surface area, and the concentration of dissolved elements in the soil solution [98], [99]. Altogether, these parameters could change the impact of biochar on soil microbes and, ultimately, on soil health.

5. Conclusion

Our results showed significant differences between the biochar produced from the tested feedstocks and at different pyrolysis temperatures. Our findings indicated that biochars produced from sludge compost are highly mineral (low organic content) and contain elements of concern. Therefore, they should be avoided (or used sparsely) to prevent soil contamination. Curiously, the biochars produced from the invasive *Prosopis juliflora* (mesquite plants) woody biomass strongly inhibited soil microbes, especially fungi. While this antimicrobial activity is unwelcome for preserving and stimulating soil health, several applications for this material can be envisioned, e.g., the inhibition of soil-borne pathogens. Based both on the biochar properties and their impact on soil microbes, pyrolysis temperatures of 450 °C appear to produce biochar with low stability, while pyrolysis temperatures of 750 °C appear to cause biotoxicity, irrespective of the feedstock type. The biochar obtained from date palm leaves at the pyrolysis temperature of 600 °C was the most promising (lower impact in soil microbes, high organic content, surface area, cation exchange capacity and thermostability) and was selected to be further tested as an amendment for agronomic soil management. Given the high variability of properties of biochar, a comprehensive understanding of biochar properties via various assessment approaches is required to establish their feasibility for specific applications. Due to the arid climate, Omani soils have low organic matter content and are often saline. The only downside of applying biochars in arid land soils is that they are alkaline and may further increase the pH values of these already alkaline soils. Further work is needed to test biochar acidification pretreatments as a means to improve their amendment value for alkaline soils of dry lands. The conversion of massive waste biomass to generate biochar via the pyrolytic process offers simultaneous potential solutions for effective waste management and soil health restoration in arid farming systems.

7. References

[1] Y. Ding *et al.*, “Biochar to improve soil fertility. A review,” *Agron. Sustain. Dev.*, vol. 36, no. 2, p. 36, Jun. 2016, doi: 10.1007/s13593-016-0372-z.

[2] J. Paz-Ferreiro, H. Lu, S. Fu, A. Méndez, and G. Gascó, “Use of phytoremediation and biochar to remediate heavy metal polluted soils: a review,” *Solid Earth Discuss.*, vol. 5, no. 2, pp. 2155–2179, 2014, doi: 10.5194/sed-5-2155-2013.

[3] N. B. Jahromi, J. Lee, A. Fulcher, F. Walker, S. Jagadamma, and P. Arelli, “Effect of biochar application on quality of flooded sandy soils and corn growth under greenhouse conditions,” *Agrosystems, Geosciences & Environment*, vol. 3, no. 1, p. e20028, 2020, doi: 10.1002/agg2.20028.

[4] A. O. Adekiya *et al.*, “Effect of Biochar on Soil Properties, Soil Loss, and Cocoyam Yield on a Tropical Sandy Loam Alfisol,” *ScientificWorldJournal*, vol. 2020, p. 9391630, Feb. 2020, doi: 10.1155/2020/9391630.

[5] M. Gopal, A. Gupta, K. Shahul Hameed, N. Sathyaseelan, T. H. Khadeejath Rajeela, and G. V. Thomas, “Biochars produced from coconut palm biomass residues can aid regenerative agriculture by improving soil properties and plant yield in humid tropics,” *Biochar*, Apr. 2020, doi: 10.1007/s42773-020-00043-5.

[6] A. H. Lahori *et al.*, “Use of Biochar as an Amendment for Remediation of Heavy Metal-Contaminated Soils: Prospects and Challenges,” *Pedosphere*, vol. 27, no. 6, pp. 991–1014, Dec. 2017, doi: 10.1016/S1002-0160(17)60490-9.

[7] S.-H. Jien and C.-S. Wang, “Effects of biochar on soil properties and erosion potential in a highly weathered soil,” *CATENA*, vol. 110, pp. 225–233, Nov. 2013, doi: 10.1016/j.catena.2013.06.021.

[8] X. Guo, H. Liu, and J. Zhang, “The role of biochar in organic waste composting and soil improvement: A review,” *Waste Management*, vol. 102, pp. 884–899, Feb. 2020, doi: 10.1016/j.wasman.2019.12.003.

[9] D. Fischer and B. Glaser, *Synergisms between Compost and Biochar for Sustainable Soil Amelioration*. IntechOpen, 2012. doi: 10.5772/31200.

[10] H. Schulz and B. Glaser, “Effects of biochar compared to organic and inorganic fertilizers on soil quality and plant growth in a greenhouse experiment,” *Journal of Plant Nutrition and Soil Science*, vol. 175, no. 3, pp. 410–422, 2012, doi: 10.1002/jpln.201100143.

[11] X. J. Lee, L. Y. Lee, S. Gan, S. Thangalazhy-Gopakumar, and H. K. Ng, “Biochar potential evaluation of palm oil wastes through slow pyrolysis: Thermochemical characterization and pyrolytic kinetic studies,” *Bioresour Technol*, vol. 236, pp. 155–163, Jul. 2017, doi: 10.1016/j.biortech.2017.03.105.

[12] E. Cárdenas- Aguiar, G. Gascó, J. Paz-Ferreiro, and A. Méndez, “The effect of biochar and compost from urban organic waste on plant biomass and properties of an artificially copper polluted soil,” *International Biodeterioration & Biodegradation*, vol. 124, pp. 223–232, Oct. 2017, doi: 10.1016/j.ibiod.2017.05.014.

[13] W. Ding, X. Dong, I. M. Ime, B. Gao, and L. Q. Ma, “Pyrolytic temperatures impact lead sorption mechanisms by bagasse biochars,” *Chemosphere*, vol. 105, pp. 68–74, Jun. 2014, doi: 10.1016/j.chemosphere.2013.12.042.

[14] P. R. Yaashikaa, P. S. Kumar, S. Varjani, and A. Saravanan, “A critical review on the biochar production techniques, characterization, stability and applications for circular bioeconomy,” *Biotechnology Reports*, vol. 28, p. e00570, Dec. 2020, doi: 10.1016/j.btre.2020.e00570.

[15] A. Tomczyk, Z. Sokołowska, and P. Boguta, “Biochar physicochemical properties: pyrolysis temperature and feedstock kind effects,” *Rev Environ Sci Biotechnol*, vol. 19, no. 1, pp. 191–215, Mar. 2020, doi: 10.1007/s11157-020-09523-3.

[16] M. Keiluweit, P. S. Nico, M. G. Johnson, and M. Kleber, “Dynamic Molecular Structure of Plant Biomass-Derived Black Carbon (Biochar),” *Environ. Sci. Technol.*, vol. 44, no. 4, pp. 1247–1253, Feb. 2010, doi: 10.1021/es9031419.

[17] J.-H. Kwak *et al.*, “Biochar properties and lead(II) adsorption capacity depend on feedstock type, pyrolysis temperature, and steam activation,” *Chemosphere*, vol. 231, pp. 393–404, Sep. 2019, doi: 10.1016/j.chemosphere.2019.05.128.

[18] N. A. de Figueredo, L. M. da Costa, L. C. A. Melo, E. A. Siebeneichlerd, and J. Tronto, “Characterization of biochars from different sources and evaluation of release of nutrients and contaminants1,” *Rev. Ciênc. Agron.*, vol. 48, pp. 3–403, Sep. 2017, doi: 10.5935/1806-6690.20170046.

[19] J. W. Gabhane, V. P. Bhange, P. D. Patil, S. T. Bankar, and S. Kumar, “Recent trends in biochar production methods and its application as a soil health conditioner: a review,” *SN Appl. Sci.*, vol. 2, no. 7, p. 1307, Jun. 2020, doi: 10.1007/s42452-020-3121-5.

[20] S. P. Sohi, E. Krull, E. Lopez-Capel, and R. Bol, “A Review of Biochar and Its Use and Function in Soil,” in *Advances in Agronomy*, vol. 105, Elsevier, 2010, pp. 47–82. doi: 10.1016/S0065-2113(10)05002-9.

[21] Y. Li *et al.*, “Effects of biochar application in forest ecosystems on soil properties and greenhouse gas emissions: a review,” *J Soils Sediments*, vol. 18, no. 2, pp. 546–563, Feb. 2018, doi: 10.1007/s11368-017-1906-y.

[22] P. Grutzmacher, A. P. Puga, M. P. S. Bibar, A. R. Coscione, A. P. Packer, and C. A. de Andrade, “Carbon stability and mitigation of fertilizer induced N2O emissions in soil amended with biochar,” *Science of The Total Environment*, vol. 625, pp. 1459–1466, Jun. 2018, doi: 10.1016/j.scitotenv.2017.12.196.

[23] S. S. Akhtar, M. N. Andersen, and F. Liu, “Biochar Mitigates Salinity Stress in Potato,” *Journal of Agronomy & Crop Science*, vol. 201, no. 5, p. 368, Oct. 2015.

[24] Y. Al-Mulla and H. M. Al-Gheilani, “Increasing water productivity enhances water saving for date palm cultivation in Oman,” *Jour. Agri. & Mar. Scie.*, vol. 22, pp. 87–91, 2017.

[25] M. Chandrasekaran and A. H. Bahkali, “Valorization of date palm (Phoenix dactylifera) fruit processing by-products and wastes using bioprocess technology – Review,” *Saudi Journal of Biological Sciences*, vol. 20, no. 2, pp. 105–120, Apr. 2013, doi: 10.1016/j.sjbs.2012.12.004.

[26] E. B. Barbier, D. Knowler, J. Gwatipedza, and and S. H. Reichard, “- An economic analysis of the invasive plant problem associated with the horticulture industry in North America,” in *Invasive Plant Ecology*, CRC Press, 2013.

[27] M. Rejmánek and D. M. Richardson, “Trees and shrubs as invasive alien species – 2013 update of the global database,” *Diversity and Distributions*, vol. 19, no. 8, pp. 1093–1094, 2013, doi: 10.1111/ddi.12075.

[28] A. Grobelak, K. Czerwińska, and A. Murtaś, “7 - General considerations on sludge disposal, industrial and municipal sludge,” in *Industrial and Municipal Sludge*, M. N. V. Prasad, P. J. de Campos Favas, M. Vithanage, and S. V. Mohan, Eds. Butterworth-Heinemann, 2019, pp. 135–153. doi: 10.1016/B978-0-12-815907-1.00007-6.

[29] R. Ahmad, G. Jilani, M. Arshad, Z. A. Zahir, and A. Khalid, “Bio-conversion of organic wastes for their recycling in agriculture: an overview of perspectives and prospects,” *Ann. Microbiol.*, vol. 57, no. 4, Art. no. 4, Dec. 2007, doi: 10.1007/BF03175343.

[30] S. Jaffar Abdul Khaliq, M. Ahmed, M. Al-Wardy, A. Al-Busaidi, and B. S. Choudri, “Wastewater and sludge management and research in Oman: An overview,” *Journal of the Air & Waste Management Association*, vol. 67, no. 3, pp. 267–278, Mar. 2017, doi: 10.1080/10962247.2016.1243595.

[31] A. R. A. Usman *et al.*, “Biochar production from date palm waste: Charring temperature induced changes in composition and surface chemistry,” *Journal of Analytical and Applied Pyrolysis*, vol. 115, pp. 392–400, Sep. 2015, doi: 10.1016/j.jaap.2015.08.016.

[32] P. J. V. Soest, “Use of Detergents in the Analysis of Fibrous Feeds. II. A Rapid Method for the Determination of Fiber and Lignin,” *Journal of Association of Official Agricultural Chemists*, vol. 46, no. 5, pp. 829–835, Oct. 1963, doi: 10.1093/jaoac/46.5.829.

[33] K. Weber, S. Heuer, P. Quicker, T. Li, T. Løvås, and V. Scherer, “An Alternative Approach for the Estimation of Biochar Yields,” *Energy Fuels*, vol. 32, no. 9, pp. 9506–9512, Sep. 2018, doi: 10.1021/acs.energyfuels.8b01825.

[34] B. Singh, M. Camps-Arbestain, and J. Lehmann, *Biochar: A Guide to Analytical Methods*. Csiro Publishing, 2017.

[35] S. Rajkovich, A. Enders, K. Hanley, C. Hyland, A. R. Zimmerman, and J. Lehmann, “Corn growth and nitrogen nutrition after additions of biochars with varying properties to a temperate soil,” *Biol Fertil Soils*, vol. 48, no. 3, pp. 271–284, Apr. 2012, doi: 10.1007/s00374-011-0624-7.

[36] Z. Liu, B. Dugan, C. A. Masiello, and H. M. Gonnermann, “Biochar particle size, shape, and porosity act together to influence soil water properties,” *PLoS One*, vol. 12, no. 6, Jun. 2017, doi: 10.1371/journal.pone.0179079.

[37] A. B. Cerato and A. J. Lutenegger, “Determination of Surface Area of Fine-Grained Soils by the Ethylene Glycol Monoethyl Ether (EGME) Method,” *GTJ*, vol. 25, no. 3, pp. 315–321, Sep. 2002, doi: 10.1520/GTJ11087J.

[38] R. T. Koide, K. Petprakob, and M. Peoples, “Quantitative analysis of biochar in field soil,” *Soil Biology and Biochemistry*, vol. 43, no. 7, pp. 1563–1568, Jul. 2011, doi: 10.1016/j.soilbio.2011.04.006.

[39] G. Estefan, “Methods of Soil, Plant, and Water Analysis: A manual for the West Asia and North Africa Region: Third Edition,” Nov. 2017, Accessed: Jan. 19, 2022. [Online]. Available: https://repo.mel.cgiar.org/handle/20.500.11766/7512

[40] W. Wang *et al.*, “Biochar Application Alleviated Negative Plant-Soil Feedback by Modifying Soil Microbiome,” *Frontiers in Microbiology*, vol. 11, p. 799, 2020, doi: 10.3389/fmicb.2020.00799.

[41] C. D. Campbell, S. J. Chapman, C. M. Cameron, M. S. Davidson, and J. M. Potts, “A Rapid Microtiter Plate Method To Measure Carbon Dioxide Evolved from Carbon Substrate Amendments so as To Determine the Physiological Profiles of Soil Microbial Communities by Using Whole Soil,” *Appl Environ Microbiol*, vol. 69, no. 6, pp. 3593–3599, Jun. 2003, doi: 10.1128/AEM.69.6.3593-3599.2003.

[42] J. Sall and J. Sall, *JMP start statistics: a guide to statistics and data analysis using JMP*. Cary, NC: SAS Pub., 2014.

[43] A. Aboulkas, H. Hammani, M. El Achaby, E. Bilal, A. Barakat, and K. el Harfi, “Valorization of algal waste via pyrolysis in a fixed-bed reactor: Production and characterization of bio-oil and bio-char,” *Bioresource Technology*, vol. 243, Jun. 2017, doi: 10.1016/j.biortech.2017.06.098.

[44] G. Stella Mary, P. Sugumaran, S. Niveditha, B. Ramalakshmi, P. Ravichandran, and S. Seshadri, “Production, characterization and evaluation of biochar from pod (Pisum sativum), leaf (Brassica oleracea) and peel (Citrus sinensis) wastes,” *Int J Recycl Org Waste Agricult*, vol. 5, no. 1, pp. 43–53, Mar. 2016, doi: 10.1007/s40093-016-0116-8.

[45] N. Claoston, A. W. Samsuri, M. H. Ahmad Husni, and M. S. Mohd Amran, “Effects of pyrolysis temperature on the physicochemical properties of empty fruit bunch and rice husk biochars,” *Waste Manag Res*, vol. 32, no. 4, pp. 331–339, Apr. 2014, doi: 10.1177/0734242X14525822.

[46] S.-X. Zhao, N. Ta, and X.-D. Wang, “Effect of Temperature on the Structural and Physicochemical Properties of Biochar with Apple Tree Branches as Feedstock Material,” *Energies*, vol. 10, no. 9, Art. no. 9, Sep. 2017, doi: 10.3390/en10091293.

[47] C. Pituello *et al.*, “Characterization of chemical–physical, structural and morphological properties of biochars from biowastes produced at different temperatures,” *Journal of Soils and Sediments*, vol. 15, Apr. 2014, doi: 10.1007/s11368-014-0964-7.

[48] M. Prasad, A. Chrysargyris, N. McDaniel, N. Gruda, and N. Tzortzakis, “Plant Nutrient Availability and pH of Biochars and Their Fractions, with the Possible Use as a Component in a Growing Media,” *Agronomy*, vol. 10, p. 10, Dec. 2019, doi: 10.3390/agronomy10010010.

[49] S. Bakshi, C. Banik, and D. A. Laird, “Estimating the organic oxygen content of biochar,” *Sci Rep*, vol. 10, no. 1, p. 13082, Aug. 2020, doi: 10.1038/s41598-020-69798-y.

[50] M. I. Al-Wabel, A. Al-Omran, A. H. El-Naggar, M. Nadeem, and A. R. A. Usman, “Pyrolysis temperature induced changes in characteristics and chemical composition of biochar produced from conocarpus wastes,” *Bioresource Technology*, vol. 131, pp. 374–379, Mar. 2013, doi: 10.1016/j.biortech.2012.12.165.

[51] Y. Zhang *et al.*, “Effect of alkali metal occurrence on the pyrolysis behavior of rice straw,” *Journal of Fuel Chemistry and Technology*, vol. 49, no. 6, pp. 752–758, Jun. 2021, doi: 10.1016/S1872-5813(21)60025-7.

[52] M. K. Hossain, V. Strezov, K. Y. Chan, A. Ziolkowski, and P. F. Nelson, “Influence of pyrolysis temperature on production and nutrient properties of wastewater sludge biochar,” *Journal of Environmental Management*, vol. 92, no. 1, pp. 223–228, Jan. 2011, doi: 10.1016/j.jenvman.2010.09.008.

[53] H. Yu, Z. Zhang, Z. Li, and D. Chen, “Characteristics of tar formation during cellulose, hemicellulose and lignin gasification,” *Fuel*, vol. 118, pp. 250–256, Feb. 2014, doi: 10.1016/j.fuel.2013.10.080.

[54] S. Pradhan, A. H. Abdelaal, K. Mroue, T. Al-Ansari, H. R. Mackey, and G. McKay, “Biochar from vegetable wastes: agro-environmental characterization,” *Biochar*, vol. 2, no. 4, pp. 439–453, Dec. 2020, doi: 10.1007/s42773-020-00069-9.

[55] B. C. Chaves Fernandes *et al.*, “Impact of Pyrolysis Temperature on the Properties of Eucalyptus Wood-Derived Biochar,” *Materials*, vol. 13, no. 24, Art. no. 24, Jan. 2020, doi: 10.3390/ma13245841.

[56] W.-J. Liu, H. Jiang, and H.-Q. Yu, “Development of Biochar-Based Functional Materials: Toward a Sustainable Platform Carbon Material,” *Chem. Rev.*, vol. 115, no. 22, pp. 12251–12285, Nov. 2015, doi: 10.1021/acs.chemrev.5b00195.

[57] S. Li, V. Barreto, R. Li, G. Chen, and Y. P. Hsieh, “Nitrogen retention of biochar derived from different feedstocks at variable pyrolysis temperatures,” *Journal of Analytical and Applied Pyrolysis*, vol. 133, pp. 136–146, Aug. 2018, doi: 10.1016/j.jaap.2018.04.010.

[58] M. Hassan *et al.*, “Influences of feedstock sources and pyrolysis temperature on the properties of biochar and functionality as adsorbents: A meta-analysis,” *Science of The Total Environment*, vol. 744, p. 140714, Nov. 2020, doi: 10.1016/j.scitotenv.2020.140714.

[59] J. López-Beceiro, A. M. Díaz-Díaz, A. Álvarez-García, J. Tarrío-Saavedra, S. Naya, and R. Artiaga, “The Complexity of Lignin Thermal Degradation in the Isothermal Context,” *Processes*, vol. 9, no. 7, Art. no. 7, Jul. 2021, doi: 10.3390/pr9071154.

[60] X. Xiao, B. Chen, Z. Chen, L. Zhu, and J. L. Schnoor, “Insight into Multiple and Multilevel Structures of Biochars and Their Potential Environmental Applications: A Critical Review,” *Environ. Sci. Technol.*, vol. 52, no. 9, pp. 5027–5047, May 2018, doi: 10.1021/acs.est.7b06487.

[61] M. Ahmad *et al.*, “Effects of pyrolysis temperature on soybean stover- and peanut shell-derived biochar properties and TCE adsorption in water,” *Bioresource Technology*, vol. 118, pp. 536–544, Aug. 2012, doi: 10.1016/j.biortech.2012.05.042.

[62] M. Van de Velden, J. Baeyens, A. Brems, B. Janssens, and R. Dewil, “Fundamentals, kinetics and endothermicity of the biomass pyrolysis reaction,” *Renewable Energy*, vol. 35, no. 1, pp. 232–242, Jan. 2010, doi: 10.1016/j.renene.2009.04.019.

[63] Y. Sun *et al.*, “Tailored design of graphitic biochar for high-efficiency and chemical-free microwave-assisted removal of refractory organic contaminants,” *Chemical Engineering Journal*, vol. 398, p. 125505, Oct. 2020, doi: 10.1016/j.cej.2020.125505.

[64] G. Q. Lu, J. C. F. Low, C. Y. Liu, and A. C. Lua, “Surface area development of sewage sludge during pyrolysis,” *Fuel*, vol. 74, no. 3, pp. 344–348, Mar. 1995, doi: 10.1016/0016-2361(95)93465-P.

[65] H. Liang, L. Chen, G. Liu, and H. Zheng, “Surface morphology properties of biochars produced from different feedstocks,” Jan. 2016, pp. 1205–1208. doi: 10.2991/iccte-16.2016.210.

[66] B. B. Uzun, E. Apaydin-Varol, F. Ateş, N. Özbay, and A. E. Pütün, “Synthetic fuel production from tea waste: Characterisation of bio-oil and bio-char,” *Fuel*, vol. 89, no. 1, pp. 176–184, Jan. 2010, doi: 10.1016/j.fuel.2009.08.040.
[67] I. Ben Salem, M. El Gamal, M. Sharma, S. Hameedi, and F. M. Howari, “Utilization of the UAE date palm leaf biochar in carbon dioxide capture and sequestration processes,” *Journal of Environmental Management*, vol. 299, p. 113644, Dec. 2021, doi: 10.1016/j.jenvman.2021.113644.
[68] I. Raya Moreno, R. Cañizares, X. Domene, V. Carabassa, and J. Alcañiz, “Comparing current chemical methods to assess biochar organic carbon in a Mediterranean agricultural soil amended with two different biochars,” *Science of The Total Environment*, vol. 598, pp. 604–618, Nov. 2017, doi: 10.1016/j.scitotenv.2017.03.168.
[69] E. Goldan, V. Nedeff, I. Sandu, N. Barsan, M. Emilian, and P. Mirela, “The Use of Biochar and Compost Mixtures as Potential Organic Fertilizers,” *Revista de Chimie*, vol. 70, pp. 2192–2197, Jul. 2019, doi: 10.37358/RC.19.6.7303.
[70] R. I. Zoghlami, S. Hechmi, R. Weghlani, N. Jedidi, and M. Moussa, “Biochar Derived from Domestic Sewage Sludge: Influence of Temperature Pyrolysis on Biochars’ Chemical Properties and Phytotoxicity,” *Journal of Chemistry*, vol. 2021, p. e1818241, Sep. 2021, doi: 10.1155/2021/1818241.
[71] M. Ahmad *et al.*, “Date palm waste-derived biochar composites with silica and zeolite: synthesis, characterization and implication for carbon stability and recalcitrant potential,” *Environmental Geochemistry and Health*, vol. 41, Aug. 2019, doi: 10.1007/s10653-017-9947-0.
[72] A. Shaaban, S.-M. Se, N. M. M. Mitan, and M. F. Dimin, “Characterization of Biochar Derived from Rubber Wood Sawdust through Slow Pyrolysis on Surface Porosities and Functional Groups,” *Procedia Engineering*, vol. 68, pp. 365–371, Jan. 2013, doi: 10.1016/j.proeng.2013.12.193.
[73] C. Guizani, M. Jeguirim, S. Valin, M. Peyrot, and S. Salvador, “The Heat Treatment Severity Index: A new metric correlated to the properties of biochars obtained from entrained flow pyrolysis of biomass,” *Fuel*, vol. 244, pp. 61–68, May 2019, doi: 10.1016/j.fuel.2019.01.170.
[74] P. Jha, A. K. Biswas, B. L. Lakaria, and A. S. Rao, “Biochar in agriculture – prospects and related implications,” *Current Science*, vol. 99, no. 9, pp. 1218–1225, 2010.
[75] B. Saletnik, M. Bajcar, G. Zaguła, M. Czernicka, and C. Puchalski, “Impact of the biomass pyrolysis parameters on the quality of biocarbon obtained from rape straw, rye straw and willow chips,” vol. 5, pp. 139–143, Jun. 2016.
[76] B. Onorevoli, G. P. da Silva Maciel, M. E. Machado, V. Corbelini, E. B. Caramão, and R. A. Jacques, “Characterization of feedstock and biochar from energetic tobacco seed waste pyrolysis and potential application of biochar as an adsorbent,” *Journal of Environmental Chemical Engineering*, vol. 6, no. 1, pp. 1279–1287, Feb. 2018, doi: 10.1016/j.jece.2018.01.039.
[77] D. Rehrah *et al.*, “Production and characterization of biochars from agricultural by-products for use in soil quality enhancement,” *Journal of Analytical and Applied Pyrolysis*, vol. 108, pp. 301–309, Jul. 2014, doi: 10.1016/j.jaap.2014.03.008.
[78] M. Waqas, A. S. Aburiazaiza, R. Miandad, M. Rehan, M. A. Barakat, and A. S. Nizami, “Development of biochar as fuel and catalyst in energy recovery technologies,” *Journal of Cleaner Production*, vol. 188, pp. 477–488, Jul. 2018, doi: 10.1016/j.jclepro.2018.04.017.
[79] B. Sizirici, Y. H. Fseha, I. Yildiz, T. Delclos, and A. Khaleel, “The effect of pyrolysis temperature and feedstock on date palm waste derived biochar to remove single and multi-metals in aqueous solutions,” *Sustainable Environment Research*, vol. 31, no. 1, p. 9, Feb. 2021, doi: 10.1186/s42834-021-00083-x.
[80] X. Yang *et al.*, “Surface functional groups of carbon-based adsorbents and their roles in the removal of heavy metals from aqueous solutions: A critical review,” *Chemical Engineering Journal*, vol. 366, pp. 608–621, Jun. 2019, doi: 10.1016/j.cej.2019.02.119.

[81] R. Janu *et al.*, “Biochar surface functional groups as affected by biomass feedstock, biochar composition and pyrolysis temperature,” *Carbon Resources Conversion*, vol. 4, pp. 36–46, Jan. 2021, doi: 10.1016/j.crcon.2021.01.003.
[82] I. Kubovský, D. Kačíková, and F. Kačík, “Structural Changes of Oak Wood Main Components Caused by Thermal Modification,” *Polymers (Basel)*, vol. 12, no. 2, p. 485, Feb. 2020, doi: 10.3390/polym12020485.
[83] B. Gámiz, K. Hall, K. A. Spokas, and L. Cox, “Understanding Activation Effects on Low-Temperature Biochar for Optimization of Herbicide Sorption,” *Agronomy*, vol. 9, no. 10, Art. no. 10, Oct. 2019, doi: 10.3390/agronomy9100588.
[84] Ö. Özgenç, S. Durmaz, I. H. Boyaci, and H. Eksi-Kocak, “Determination of chemical changes in heat-treated wood using ATR-FTIR and FT Raman spectrometry,” *Spectrochim Acta A Mol Biomol Spectrosc*, vol. 171, pp. 395–400, Jan. 2017, doi: 10.1016/j.saa.2016.08.026.
[85] L. Leng, H. Huang, H. Li, J. Li, and W. Zhou, “Biochar stability assessment methods: A review,” *Science of The Total Environment*, vol. 647, pp. 210–222, Jan. 2019, doi: 10.1016/j.scitotenv.2018.07.402.
[86] Y. Sun *et al.*, “Effects of feedstock type, production method, and pyrolysis temperature on biochar and hydrochar properties,” *Chemical Engineering Journal*, vol. 240, pp. 574–578, Mar. 2014, doi: 10.1016/j.cej.2013.10.081.
[87] W. Wang *et al.*, “Pyrolysis temperature and feedstock alter the functional groups and carbon sequestration potential of Phragmites australis - and Spartina alterniflora -derived biochars,” *GCB Bioenergy*, vol. 13, Mar. 2021, doi: 10.1111/gcbb.12795.
[88] S. Li and G. Chen, “Thermogravimetric, thermochemical, and infrared spectral characterization of feedstocks and biochar derived at different pyrolysis temperatures,” *Waste Management*, vol. 78, pp. 198–207, Aug. 2018, doi: 10.1016/j.wasman.2018.05.048.
[89] A. Ameen, A. Saeed, N. Yub Harun, M. Nasef, and N. Yub, “Physicochemical Characterization of Different Agricultural Residues in Malaysia for Bio-Char Production,” *International Journal of Civil Engineering and Technology*, vol. 10, pp. 213–225, Oct. 2019.
[90] M. Jeguirim and L. Limousy, *Biomass Chars: Elaboration, Characterization and Applications*. MDPI, 2018.
[91] M. Azeem *et al.*, “Effects of biochar and NPK on soil microbial biomass and enzyme activity during 2 years of application in the arid region,” *Arab J Geosci*, vol. 12, no. 10, p. 311, May 2019, doi: 10.1007/s12517-019-4482-1.
[92] Z. Dai *et al.*, “Association of biochar properties with changes in soil bacterial, fungal and fauna communities and nutrient cycling processes,” *Biochar*, vol. 3, no. 3, pp. 239–254, Sep. 2021, doi: 10.1007/s42773-021-00099-x.
[93] J. L. Deenik, T. McClellan, G. Uehara, M. J. Antal, and S. Campbell, “Charcoal Volatile Matter Content Influences Plant Growth and Soil Nitrogen Transformations,” *Soil Science Society of America Journal*, vol. 74, no. 4, pp. 1259–1270, 2010, doi: 10.2136/sssaj2009.0115.
[94] Y. Luo, M. Durenkamp, M. De Nobili, Q. Lin, B. J. Devonshire, and P. C. Brookes, “Microbial biomass growth, following incorporation of biochars produced at 350 °C or 700 °C, in a silty-clay loam soil of high and low pH,” *Soil Biology and Biochemistry*, vol. 57, pp. 513–523, 2013, doi: 10.1016/j.soilbio.2012.10.033.
[95] A. Cross and S. P. Sohi, “The priming potential of biochar products in relation to labile carbon contents and soil organic matter status,” *Soil Biology and Biochemistry*, vol. 43, no. 10, pp. 2127–2134, Oct. 2011, doi: 10.1016/j.soilbio.2011.06.016.
[96] X. Chen *et al.*, “Adsorption of copper and zinc by biochars produced from pyrolysis of hardwood and corn straw in aqueous solution,” *Bioresource Technology*, vol. 102, no. 19, pp. 8877–8884, Oct. 2011, doi: 10.1016/j.biortech.2011.06.078.
[97] N. Xu, G. Tan, H. Wang, and X. Gai, “Effect of biochar additions to soil on nitrogen leaching, microbial biomass and bacterial community structure,” *European Journal of Soil Biology*, vol. 74, pp. 1–8, May 2016, doi: 10.1016/j.ejsobi.2016.02.004.

[98] C. Bamminger, N. Zaiser, P. Zinsser, M. Lamers, C. Kammann, and S. Marhan, “Effects of biochar, earthworms, and litter addition on soil microbial activity and abundance in a temperate agricultural soil,” *Biol Fertil Soils*, vol. 50, no. 8, pp. 1189–1200, Nov. 2014, doi: 10.1007/s00374-014-0968-x.

[99] K. N. Palansooriya *et al.*, “Response of microbial communities to biochar-amended soils: a critical review,” *Biochar*, vol. 1, no. 1, pp. 3–22, Mar. 2019, doi: 10.1007/s42773-019-00009-2.